Hindawi
Shock and Vibration
Volume 2021, Article ID 5574696, 12 pages
https://doi.org/10.1155/2021/5574696

Research Article

Testing Method for the Range of Fracture Zone of Rock Slope under Blasting Load

Zhide Wang,[1] Zuyao Ma,[1] Yuanyou Xia,[1] Xiong Zhou,[1] Manqing Lin,[2] Jie Li,[1] and Jinyuan Wang [1,3]

[1]*School of Civil Engineering and Architecture, Wuhan University of Technology, Wuhan 430070, China*
[2]*Engineering Research Center of Phosphorus Resources Development and Utilization of Ministry of Education, Wuhan Institute of Technology, Wuhan 430205, China*
[3]*State Key Laboratory of Water Resources and Hydropower Engineering Science, Wuhan University, Wuhan 430072, China*

Correspondence should be addressed to Jinyuan Wang; jinyuan.wang521@whut.edu.cn

Received 12 January 2021; Accepted 27 May 2021; Published 7 June 2021

Academic Editor: Qi ZHAO

In engineering blasting, the determination of the range of rock blasting fracture zone has important guiding significance for blasting construction. This paper proposes a method that can accurately and directly obtain the range of rock blasting fracture zone. Based on the theory of elastic wave propagation, test rods which are made of appropriate material are selected and prepared. A certain number of boreholes are drilled for subsequent insertion of the test rods along the direction perpendicular to the free surface of the excavation at a certain distance from the blast hole. Based on the field blasting test results, the deepest fracture position of the test rod is used as the boundary of the blasting fracture zone, and the range of the rock blasting fracture zone is obtained. A numerical analysis model is established according to the Mohr–Coulomb constitutive relationship and the Von Mises yield criterion. Then, the range of the fracture zone and the maximum horizontal radius of the fracture zone are analyzed and obtained. The numerical analysis results are compared with the field measured data. It is demonstrated that the range of the fracture zone obtained by the numerical simulation is in good agreement with the blasting test results of the pre-embedded test rods. The research results can provide references for the safety control of blasting and excavation of rock slopes.

1. Introduction

Because blasting has the merits of fast excavation speed, high efficiency, and low cost, it has been widely used in the process of rock slope excavation and open-air pit mining. However, blasting inevitably affects and damages the slope. The study of the maximum horizontal radius and range of the slope fracture zone can guide on-site blasting excavation and is of great significance to retain the integrity of the bedrock and ensure the engineering safety. It is also a problem that the engineering community is generally concerned about. When the explosive is buried adjacent to the ground free surface, the phenomenon of rupture, bulging, and throwing will occur according to the distance between the explosion center and the free surface. Livingston [1] divided the explosive depth into four zones. When the explosive depth is in the impact damage zone, the surface rocks exhibit bulging and throwing, forming a blasting funnel. According to different blasting action indexes, the blasting funnel can be divided into four forms, i.e., standard throwing blasting funnel, strengthened throwing blasting funnel, weakened throwing blasting funnel, and loosened blasting funnel. When the explosive explodes in the blast hole, a high-strength dynamic stress wave will be formed on the surface of the rock outside the blast hole, and then the stress wave will propagate as an elastic wave in the surrounding rocks, producing crushing zones, fracture zones, and vibration zones [2]. Research [3, 4] showed that the radius of the crushed circle is about 2~3 times the charging radius, but the results of the research on the relationship between the radius of the fracture zone and the charging radius are controversial.

Regarding the theoretical description of the damage caused by explosive loads to rock masses, it is currently mainly quantified by damage variables. Researchers have made certain progress in this regard. For example, Taylor et al. [5, 6] have defined damage variables of rock by describing the statistical distribution characteristics of fractures and established the corresponding damage model. Chen et al. [7–10] further customized the damage variables, established a damage model that considers the integrity of the rock mass, and conducted a research on the range of blasting damage. At present, the widely used damage models include Taylor–Chen–Kuszmaul (TCK) model and YANG model [11, 12]. The research on the range of blasting damage is often carried out by a combination of field test and numerical analysis [13]. In the aspect of field testing, testing methods such as rock drilling acoustic wave testing and borehole television are widely used to determine the range of damage and tend to be convenient and efficient [14–18]. However, the acoustic wave test method requires water as a coupling agent, while the accuracy of the borehole television method needs to be further improved. Both methods need to reserve holes in advance, which is not necessarily required in actual blasting shock wave propagation. In terms of numerical analysis, numerical software such as ANSYS/LS-DYNA and FLAC3D is generally used. Based on the Von Mises yield criterion, tensile stress failure criterion, or compressive stress failure criterion in the rock, the range of blasting damage is determined by adopting equivalent explosion load, appropriate blasting geometric model, and constitutive model, combined with actual boundary conditions and initial conditions [19, 20]. Pan et al. [21] believed that there is a free-surface blasting, and the failure mode of the rock is mainly tensile failure. The Von Mises yield criterion is used as the basis for rock failure under blasting load, and the optimal hole bottom distance and minimum resistance line are obtained. Li et al. [19] determined the range of blasting damage according to the effective stress in the rock, which turns out relatively accurate. Although the related research is much, due to the complicated generation mechanism and evolution law of the blasting fracture zone, there are visible differences in the range of the fracture zone obtained. Moreover, there are relatively few studies on the practical application of the theory that describes stress wave propagation through the interface between different media.

On the basis of previous research results, this paper attempts to propose a more accurate and intuitive test method to determine the range of rock blasting fracture zone. In the area near the blast hole, the pre-embedded test rod was drilled along the direction perpendicular to the free surface of the excavation. The rupture depth of each test rod at different positions from the blast hole was obtained through the field blasting test, and the range of the rock fracture zone under the blasting load was obtained. The results will provide construction references for safe blasting excavation of rock slopes.

2. Test Method and Principle

2.1. Test Method. According to the wave impedance, compressive strength, and dynamic compressive strength of the rock at the test site, the appropriate test rod material is selected and test rods with similar materials are prepared in the laboratory. The ratio of the dynamic compressive strength of the test rod to the dynamic tensile strength of the rock is required to be close to the transmission coefficient of the stress wave at the interface between the test rod and rock. The transmission coefficient is determined by the ratio of the wave impedance of the test rod material to the rock.

At a certain distance from the blast hole, each test hole is drilled along the direction perpendicular to the free surface of the excavation. The test holes have the same depth as that of the blast hole and are numbered in an increasing order with the distance from the blast hole. The prepared test rods are numbered accordingly based on their respective test holes. The diameter of the test hole and blast hole drilled by the field drill is slightly larger than the diameter of the test rod. After each test rod is placed into the test hole separately, the gap between them is filled with gravel so that the test rod is in close contact with the original rock. After blasting, the maximum rupture range of the test rod is taken as the range of blasting fracture zone of the rock.

2.2. Test Principle. The rock is in a three-dimensional stress state of tension and compression. Due to the impact load, the surrounding rock is in a strongly compressed state. The explosive stress is much greater than the dynamic compressive strength of the rock. Subjected to the great explosive stress and the action of the high temperature and high pressure produced by the explosive gas, the rock is crushed. Outside the crushing zone, the explosive stress in the rock is less than the dynamic compressive strength of the rock and the tensile stress generated in the rock is greater than the dynamic tensile strength of the rock. As a result, the rock is subjected to tensile failure [4]. The Von Mises yield criterion is used to approximately judge whether the rock is damaged [21]. Radial stress σ_r and tangential stress σ_θ at any point in the rock are as shown in Figure 1 [22]. The sign rule is according to the convention which considers the tension positive. The stress at any point in the rock can be expressed as follows:

$$|\sigma_i| = \sqrt{\frac{(\sigma_r - \sigma_\theta)^2 + (\sigma_\theta - \sigma_z)^2 + (\sigma_z - \sigma_r)^2}{2}}, \quad (1)$$

where σ_i is Von Mises stress (MPa); σ_r is the radial stress in the rock (MPa); σ_θ is the tangential stress in the rock (MPa); and σ_z is the normal stress along the longitudinal axis of the blast hole (MPa).

According to the Von Mises criterion, there are inequalities expressed by equation (2). When the stress at any

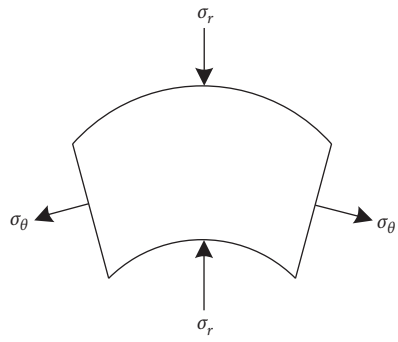

Figure 1: Stress state at any point in the rock mass.

point in the rock satisfies equation (2), the rock will be damaged [4].

$$|\sigma_i| \geq \begin{cases} \sigma_{td} \text{ (fractured circle)}, \\ \sigma_{cd} \text{ (crushed circle)}, \end{cases} \tag{2}$$

where σ_{td} is the dynamic tensile strength of the rock (MPa) and σ_{cd} is the dynamic compressive strength of the rock (MPa). The dynamic tensile strength of the rock is generally determined by $\sigma_{td} = (4 \sim 8)\sigma_t$, where σ_t is the static tensile strength of the rock. The dynamic compressive strength of rock increases with the increase in the loading strain rate [4]:

$$\sigma_{cd} = \sigma_c \dot{\varepsilon}^{(1/3)}, \tag{3}$$

where σ_c is the static compressive strength of the rock (MPa) and $\dot{\varepsilon}$ is the loading strain rate of the rock (s^{-1}).

As shown in Figure 2, when the explosive stress wave passes through the interface between the test rod and the rock, reflection and transmission occur. When an elastic stress wave is transmitted from one medium to another medium, the reflection and transmission of the stress wave will occur at the interface of the two media. According to Newton's third law [4],

$$\begin{cases} \sigma_R = F\sigma_I, \\ \sigma_T = T\sigma_I, \end{cases} \tag{4}$$

where σ_R and σ_T are the reflected wave stress and the transmitted wave stress of the particles on both sides of the interface, respectively, and σ_I is the incident wave stress of the particle (MPa).

$$\begin{cases} n = \dfrac{\rho_1 c_1}{\rho_2 c_2}, \\ F = \dfrac{1-n}{1+n}, \\ T = \dfrac{2}{1+n}, \end{cases} \tag{5}$$

where F and T are the reflection coefficient and transmission coefficient, respectively; ρ_1 and ρ_2 are the densities of the original medium and the other medium (kg/m^3), respectively; c_1 and c_2 are the longitudinal wave velocities of the original medium and the other medium (m/s), respectively; and n is the ratio of the wave impedance of the two media.

Since the compressive strength of the test rod is much smaller than that of the rock on-site, the intensity of the transmitted stress wave after the explosion stress wave passes through the interface between the test rod and the rock is much greater than the dynamic compressive strength of the test rod. Therefore, the test rod will be mainly subjected to compressive failure. When the original on-site rock is at the position of the test rod, the intensity of the stress wave passed is smaller than the dynamic compressive strength of the rock. It thus cannot directly crush the rock. However, it can still damage the rock. The relatively large radial compression results in radial compressive strains and tangential tensile strains in the rock layer surrounding the crushing zone. Once the generated tangential tensile stress is greater than the dynamic tensile strength of the rock, radial cracks will be generated, which form the fracture zone. Therefore, the original rock corresponding to the rod position is mainly subjected to tensile failure.

When the ratio of the dynamic compressive strength of the test rod to the dynamic tensile strength of the rock and the ratio of the transmitted wave stress to the incident wave stress (i.e., transmission coefficient) are close, it can be considered that the fracture position of the test rod under the blasting load and its corresponding field rock is the same, so the fracture position and fracture range of the test rod can be used to judge the fracture range of the rock on-site.

3. Field Blasting Test

3.1. Project Overview. A limestone mine in Bazhong, Sichuan, is a hillside open-pit mine. The mine mainly yields limestone and flint limestone. The rock mass in the mining area has a steeply dipping layered structure. The fractures are generally developed, but the connectivity is poor, and no secondary folds and faults are seen. The integrity of the rock formation is good, and the geological structure is relatively simple. The blasting scheme adopts a top-down open-pit mining method with horizontal steps, following the principle of simultaneous mining and stripping with stripping first. The on-site blasting test was selected on a platform with an elevation of 1278 m, and the test location is shown in Figure 3. There was a certain thickness (around 5 cm) of fine gravel muck on the surface (see Figure 4), but the thickness of the top soil of the platform is negligible relative to the hole depth.

3.2. Drilling and Blasting Parameters. The field blasting test uses 2# rock emulsion explosive, and the drilling and blasting parameters are shown in Table 1. The physical and mechanical parameters of the limestone rock obtained by laboratory tests are shown in Table 2. The values of c_1 and φ_1 listed in Table 2 were obtained by triaxial compression tests on the limestone rock in natural state. The natural rock samples were tested at five confining pressures (i.e., 2 MPa, 4 MPa, 6 MPa, 8 MPa, and 10 MPa). Mohr's circles and obtained strength parameters are shown in Figure 5.

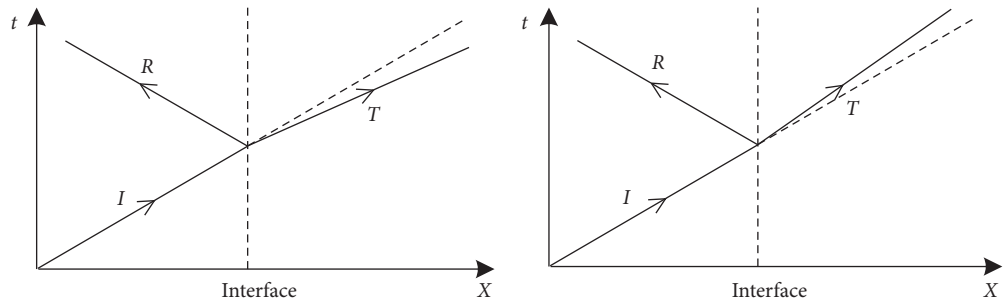

Figure 2: Reflection and transmission of elastic waves: (a) $\rho_1 c_1 < \rho_2 c_2$; (b) $\rho_1 c_1 > \rho_2 c_2$.

Figure 3: Mine test site: (a) test platform; (b) test position.

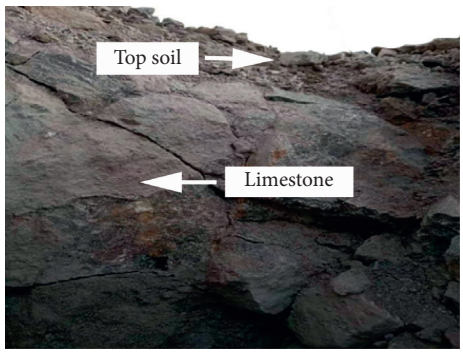

Figure 4: Photograph of the blast hole taken upward from the inside.

3.3. Parameter Determination of Test Rod. In the field blasting test, the gypsum rod was used as the test rod. The gypsum rods are prepared by mixing gypsum and water with a certain gravimetric ratio. Three kinds of gypsum rods are made by adopting water-gypsum ratios of 0.7, 1.0, and 1.3, respectively. The physical parameters of the gypsum rods with the three water-gypsum ratios are shown in Table 3.

The longitudinal wave velocity of the stress wave in the elastic medium is as follows:

$$c_0 = \sqrt{\frac{E}{\rho_0}}, \tag{6}$$

where c_0 is the longitudinal wave velocity in the medium (m/s); E is the elastic modulus of the medium (Pa); and ρ_0 is the density of the medium (kg/m^3).

In engineering blasting, the loading rate in crushed zone is high, which is taken as $\dot{\varepsilon} = 10^0 \sim 10^4\ \mathrm{s}^{-1}$. When the gypsum rod is located outside the crushed zone, the loading rate decreases further. According to the condition of the field testing, the load rate is taken as $\dot{\varepsilon} = 10^2\ \mathrm{s}^{-1}$. The dynamic compressive strength of the gypsum rod can be obtained by equation (3). From equation (6), it can be derived that the longitudinal wave velocities of the gypsum rods with water-gypsum ratios of 0.7, 1.0, and 1.3 are $c_{p0.7} = 1277.7$ m/s, $c_{p1.0} = 1149.8$ m/s, and $c_{p1.3} = 1100.6$ m/s, respectively.

The longitudinal wave velocity in the rock measured by sonic tester on-site is $c_p = 3430$ m/s. The dynamic tensile strength of the on-site rock is determined as $\sigma_{td1} = 6\sigma_t = 33.42$ MPa, in which the value of the static tensile strength σ_t is from the laboratory tensile strength test result listed in Table 2. Using equation (5), the wave impedance ratio, n, and the transmission coefficient, T, of gypsum rods with different water-gypsum ratios and the

Table 1: Drilling and blasting parameters of the field blasting test.

Blast hole diameter (cm)	Blast hole depth (m)	Dose (kg)	Blockage length (cm)
14	2	10	40

Table 2: Physical and mechanical parameters of the limestone rock.

Elastic modulus E_1 (GPa)	Poisson's ration μ_1	Density ρ_1 (kg · m^{-3})	Internal friction angle φ_1 (°)	Cohesion c_1 (MPa)	Tensile strength σ_t (MPa)
38.5	0.296	2680	55	16.25	5.57

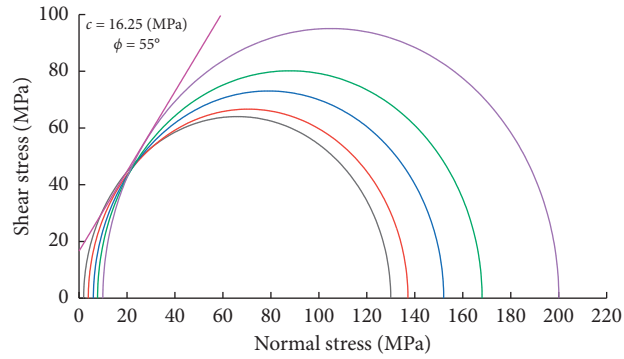

Figure 5: Compressive strength parameters of limestone rock samples in natural state.

original rock at the contact surface can be obtained. The ratio of the dynamic compressive strength of the gypsum rod to the dynamic tensile strength of the rock can be then calculated. The calculation results are tabulated in Table 4.

It can be seen from Table 4 that when the ratio of water to gypsum is 1.0, the transmission coefficient T is 0.247, which is close to the ratio of the dynamic compressive strength of the gypsum rod to the dynamic tensile strength of the rock $\sigma_{cd2}/\sigma_{td1} = 0.229$. Therefore, the gypsum rod with a water-gypsum ratio of 1.0 is selected for field testing.

The preparation procedure of the test rod is as follows. (1) A PVC pipe with a length of 1.0 m and an inner diameter of 0.14 m was cut and split into two halves along the center line. After brushing a layer of oil on the inner side of the pipe, it was then wounded with adhesive tape for bonding. (2) One end of the PVC pipe was sealed, and an iron wire was fastened at the center of sealed end. (3) Gypsum slurry was then poured into the PVC pipe. When grouting, the iron wire was kept in a centered and tensed state, while vibrating and stirring until the gypsum was uniformly formed. (4) The gypsum rods were taken out and cured naturally for 7 days. Two 1.0 m length gypsum rods are connected to a 2.0 m long gypsum rod through the embedded iron wire.

3.4. Blasting Test. At a distance of 1.0 m from the blast hole, test holes were drilled along the direction perpendicular to the free surface near the excavation. In the field blasting test, the orientation angle of the connection line between the blast hole and the nearest test hole is 60°. The test hole spacing is 0.6 m. Before the test, the prepared gypsum rods were numbered 1~4 according to their distances from blast hole from the near to the distant. The diameter of the gypsum rod was 0.14 m, and the test holes and blast hole were all 2.0 m deep. The layout of the on-site shallow hole blasting test is shown in Figure 6, and the gypsum rods before the blasting test are shown in Figure 7.

3.5. Result Analysis. After the field blasting test, the free-surface fracture zone on the top of the blast hole is shown in Figure 8, and the rupture range of the gypsum rod is shown in Figure 9.

It can be seen from Figure 8 that the explosive center with a burial depth of 1.2 m is in the impact damage zone, forming a loose blasting funnel [1], and bulging occurs on the slope surface. The longest radial fracture length measured on-site is 3.16 m, which is about 20 times the radius of the blast hole. The distance from the circumferential fracture closest to the blast hole to the circumference of the blast hole measured on-site is 0.224 m, which is about 3 times the radius of the blast hole. Therefore, the field test results conform to the general blasting law.

In Figure 9(a), the gypsum rods are No. 1~4 in order from right to left. Since the No. 1 and No. 2 gypsum rods are very close to the blast hole and most affected by the blasting, the lower half parts stuck in the test hole and were not extracted. The measurements of rupture position are shown in Figure 9(b). It can be seen from Figure 9 that the fracture depth of No. 3 gypsum rod is 1.445 m, and the upper part is broken; the fracture depth of No. 4 gypsum rod is 0.3 m. Because there is a fracture in the lower part of No. 3 gypsum rod and the No. 1 and No. 2 gypsum rods are closer to the blast hole, it can be inferred that there are fractures in both upper and lower parts for No. 1 and No. 2 gypsum rods. According to the fracture depth of each gypsum rod, it can be concluded that the fracture depth of the gypsum rod decreases with the increase in the distance from the explosion center during the blasting process, and the rock fracture range is funnel-shaped.

4. Numerical Simulation

The combination of field test and numerical analysis can more accurately reproduce the damage range of the rock under the blasting load. Therefore, the numerical analysis is conducted to further validate the accuracy of using test rod to obtain the fracture range of the original rock on-site under the blasting load.

Table 3: The physical parameters of the gypsum rods with different water-gypsum ratios.

Water-gypsum ratio	Elastic modulus E_2 (GPa)	Poisson's ratio μ_2	Density ρ_2 (kg · m^{-3})	Compressive strength σ_c (MPa)
0.7	2.31	0.250	1408.8	4.08
1.0	1.49	0.198	1127.1	1.65
1.3	1.23	0.169	1015.4	1.25

Table 4: Calculated parameters of the original rock and test rods with different water-gypsum ratios.

Water-gypsum ratio	Wave impedance ratio n	Transmission coefficient T	Dynamic compressive strength σ_{cd2} (MPa)	$\sigma_{cd2}/\sigma_{td1}$
0.7	5.10	0.327	18.930	0.566
1.0	7.09	0.247	7.656	0.229
1.3	8.20	0.217	5.800	0.173

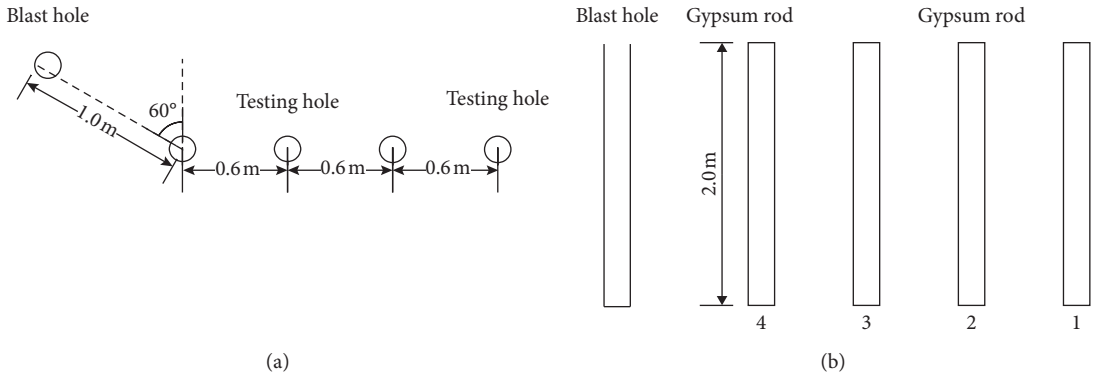

Figure 6: Schematic diagram of the field blasting test: (a) plan view; (b) sectional view.

Figure 7: Gypsum rod before the blasting test.

4.1. Blasting Load. The Chapmam–Jouguet (C-J) theory can qualitatively explain the physical phenomenon of explosive detonation. The C-J model of detonation regards the detonation surface as a sudden interface [4] between the explosive without thickness and the reactant. Under C-J conditions, the average instantaneous detonation pressure of condensed explosive, P_0, is expressed as follows:

$$P_0 = \frac{\rho_0 D_0^2}{\gamma + 1}, \tag{7}$$

where ρ_0 is the explosive density; D_0 is the explosive velocity; γ is a constant related to the properties of condensed explosives and charge density, and the value is 2~3. For 2# rock emulsion explosive, take $\rho_0 = 1200\,\text{kg/m}^3$, $D_0 = 3600\,\text{m/s}$, and $\gamma = 3$.

The peak shock pressure, P_b, is expressed as follows:

$$P_b = \frac{2\rho c_p}{\rho c_p + \rho_0 D_0} P_0, \tag{8}$$

where ρ is the rock density (kg/m^3) and c_p is the measured longitudinal wave velocity in the rock, $c_p = 3430\text{m/s}$.

The field blasting test adopts a coupled charge structure and uses a triangular load to approximate the blasting load. The impact pressure loading curve on the blast hole wall can be simplified to a triangular loading curve, as shown in Figure 10.

The explosion load increases rapidly at the moment of blasting, assuming the rise time of the explosion load t_r equals to the propagation time of the detonation wave [23], namely:

$$t_r = \frac{L_1}{D_0}, \tag{9}$$

where L_1 is the length of the charge.

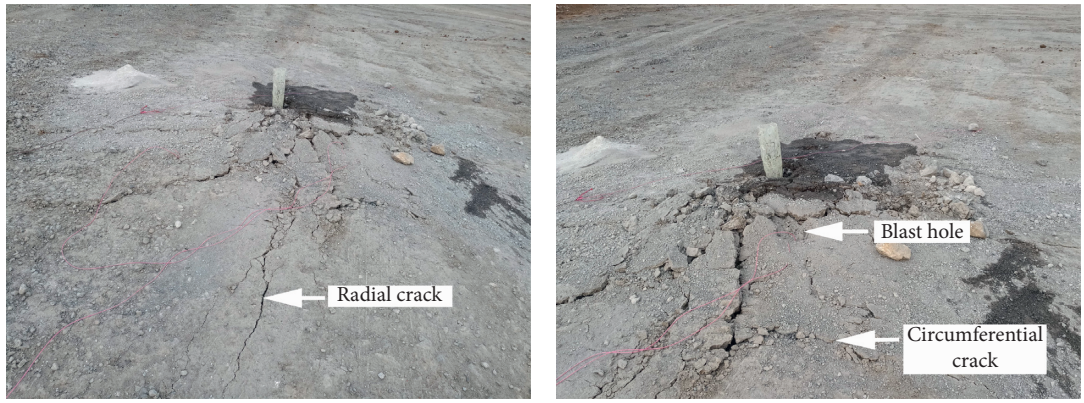

Figure 8: Fracture diagram after the blasting test: (a) radial crack; (b) circumferential crack.

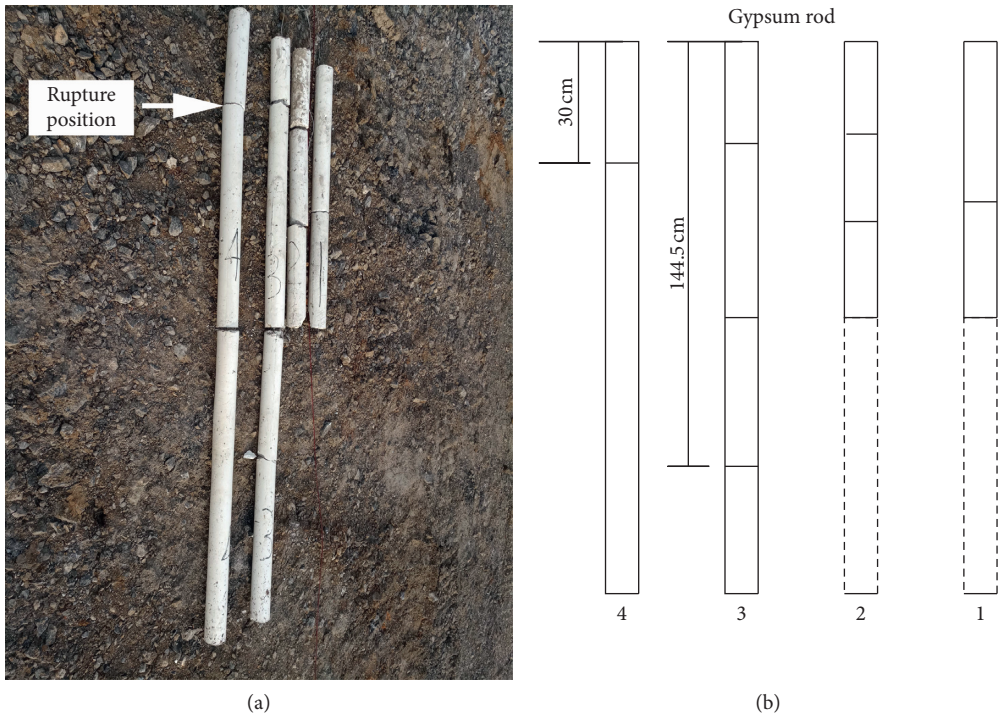

Figure 9: Gypsum rod after the blasting test: (a) field observation; (b) measured data.

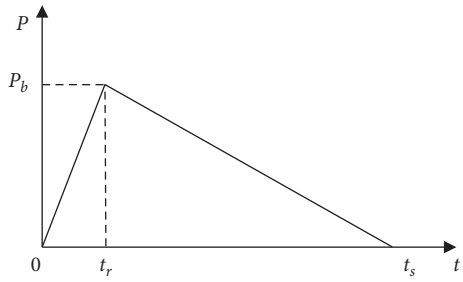

Figure 10: Equivalent diagram of blasting load.

The ratio of the rise time to the total action time of the commonly used triangular explosion load [23] is 1: $7Q^{0.15}$ (Q is the charge dosage; see Table 1). The total action time of the explosion load t_s can be obtained by the following equation:

$$t_s = 7Q^{0.15}t_r. \tag{10}$$

Calculated by equations (9) and (10), the rise time of the on-site gypsum rod test load is $t_r = 0.5$ ms. The total load time is $t_s = 5.0$ ms.

4.2. Calculation Model

4.2.1. Constitutive Model. Assuming that the rock is an isotropic material, the Mohr–Coulomb constitutive model is adopted in this work to analyze the constitutive stress-strain relationship of rock materials.

4.2.2. Model Size and Boundary Conditions. In order to simplify the calculation, a 1/4 cylinder is taken as the calculation model based on the symmetry. In order to reduce the influence of the model boundary, based on the size of the crushing zone and the fracture zone produced by rock blasting, the 1/4 cylinder with the radius of 8.0 m and the height of 8.0 m is used as the model for simulating the field blasting. The blast hole radius is set to be 0.07 m according to the actual on-site geometry. The vertical boundary of the model restricts the horizontal displacement. The lower boundary restricts the vertical displacement. The circumferential boundary adopts a static viscous boundary to reduce the influence of boundary reflection waves on the calculation results. The top horizontal plane is set as the free surface, and the particle velocity on each boundary in the initial state is set to be 0.

4.2.3. Damping. In the dynamic analysis with large strain, simply setting a very small damping ratio can meet the requirements. Rayleigh damping [3] is selected in this work, and its value is set to be 0.005.

4.2.4. Meshing. The size of the grid element has a great effect on the numerical simulation results. To reach decent accuracy, the following relationship [3] must be satisfied:

$$\Delta l \leq \left(\frac{1}{8} \sim \frac{1}{10}\right)\lambda, \tag{11}$$

where Δl is the grid size and λ is the wavelength corresponding to the highest frequency f that signifies appreciable energy, $\lambda = c/f$, where c is the corresponding wave velocity.

Blasting vibration velocity waveforms and dominant frequencies were obtained by employing the blasting vibration tester (UBOX-5016; see Figure 11). The on-site blasting vibration velocity waveforms in horizontal radial, horizontal tangential, and vertical directions are shown in Figure 12.

It can be seen from Figure 12 that the maximum dominant frequency in three directions is $f_m = 29.907$ Hz, which approximately represents the highest frequency f. The corresponding wave velocity c is approximately represented by the longitudinal wave velocity c_p of the rock, which is $c_p = 3430$ m/s as measured. The wavelength is then obtained, $\lambda \approx c_p/f_m = 114.7$ m. According to equation (11), $\Delta l \leq (1/8 \sim 1/10)$ and $\lambda = (11 \sim 14$ m).

The cylindrical shell modeling method is adopted. The inner and outer radii of the shell are 0.07 m and 8.0 m, respectively. The number of grid elements in the radial direction is 20, and the size of the individual grid is increased by a ratio of 1.1 from center outward. The vertical plane is evenly divided into 10 grid elements within a depth of 2 m. In the depth range below 2 m, the size of the individual grid is increased downward by the ratio of 1.05. The centripetal part of the shell below the depth of 2 m is filled. The counterpart within the depth of 2 m is not filled to reserve the blast hole. The radius of the filling part is 0.07 m. The number of grids in the radial direction is 2, and the mesh division method is the same as that of the shell below the depth of 2 m. At the same time, the annulus sector is equally divided into 30 parts. The portions closer to the blast hole are divided more densely so as to ensure the accuracy of the calculation results and reduce the calculation convergence time. The minimum size of the model mesh is 0.03 m, and the maximum mesh size is 0.85 m. The numerical analysis model is shown in Figure 13. The red part is the blast hole.

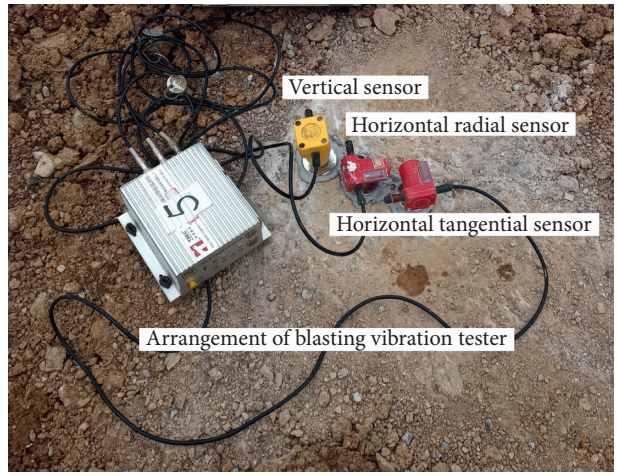

Figure 11: The arrangement of on-site blasting vibration tester.

4.3. Result Analysis.

The Von Mises yield criterion is used as the rock failure criterion to depict the rock fracture zone in the numerical analysis. Figures 14 and 15 show the evolution process with time of the rock fracture zone in the horizontal and vertical planes, respectively.

It can be seen from Figures 14 and 15 that the fracture range of the rock under the blasting load increases with time. After 3.0 ms, the fracture range is basically unchanged, and the stress generated by blasting gradually attenuates. Therefore, the numerical analysis result at 3.0 ms is taken as the range of the rock fracture zone. The comparison of the numerical analysis and the measured results is shown in Figure 16.

It can be seen from Figure 16 that the fracture depths of No. 1~4 gypsum rods are 2.353 m, 2.161 m, 1.572 m, and 0.354 m, respectively. The measured fracture depths of No. 3 and No. 4 gypsum rods are close to the numerical analysis results, and the relative error between the numerical analysis results and the measured results of the gypsum rods is not more than 18%, which meets the requirements of engineering accuracy. At the same time, the fracture depths corresponding to No. 1 and No. 2 gypsum rods from the numerical analysis are both greater than 2.0 m, indicating

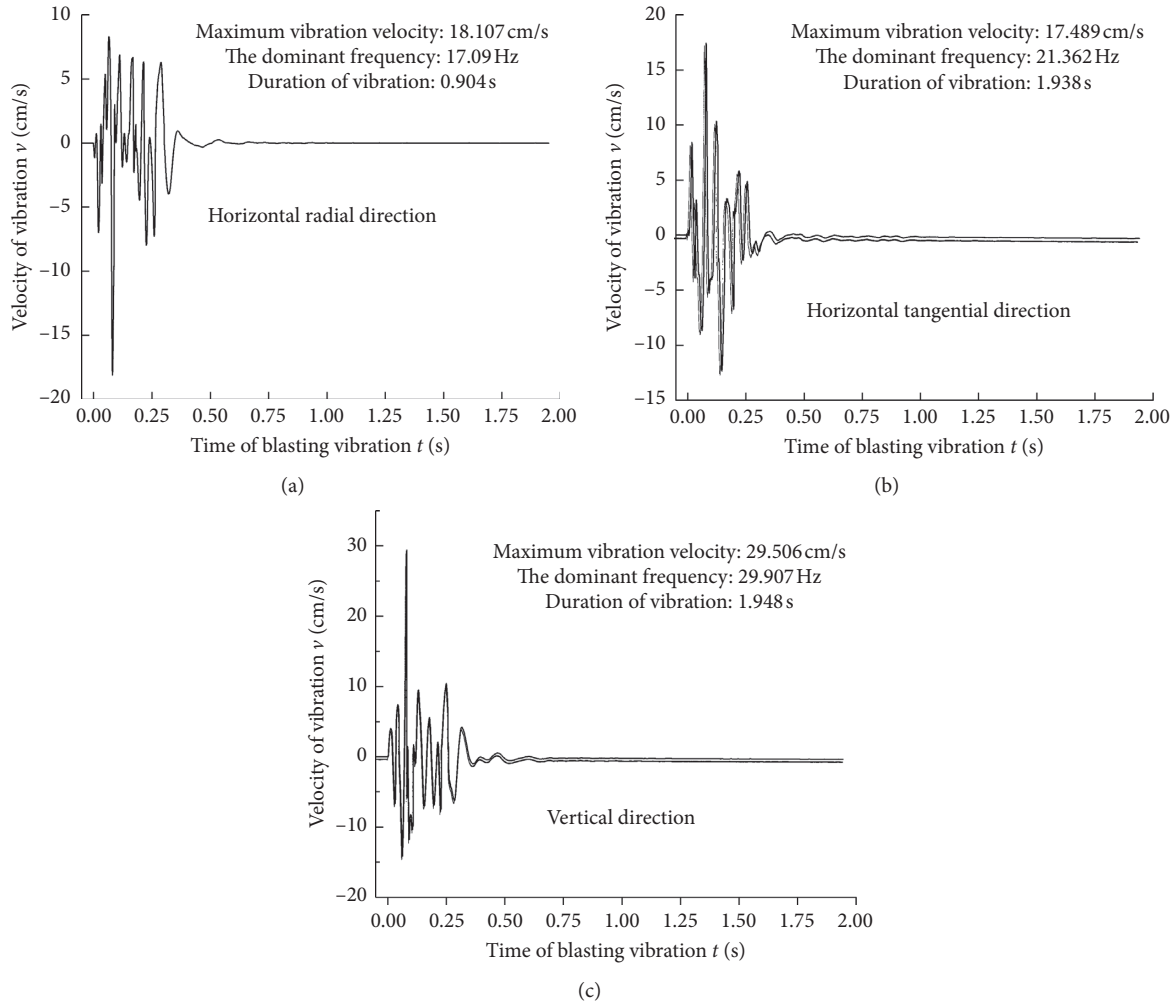

Figure 12: Field blasting vibration test results: (a) horizontal radial vibration of the particle; (b) horizontal tangential vibration of the particle; (c) vertical vibration of the particle.

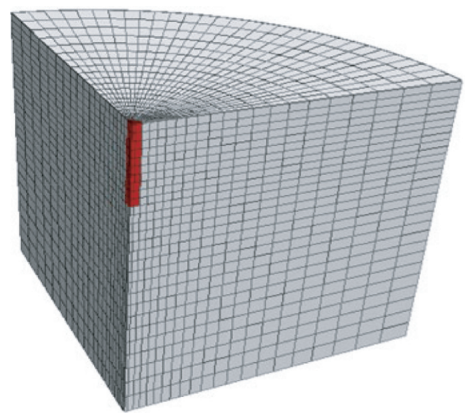

Figure 13: The meshing diagram of the numerical model.

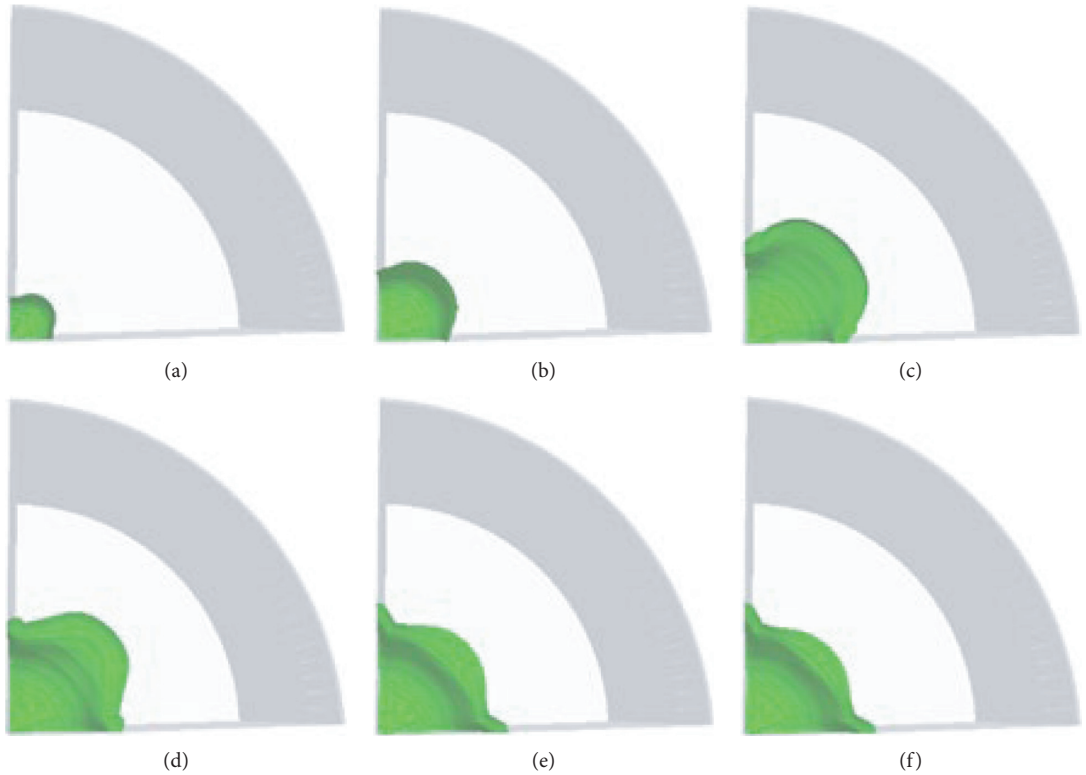

Figure 14: The development of rock mass fracture zone in bird's-eye view: (a) 0.5 ms; (b) 0.8 ms; (c) 1.5 ms; (d) 2.0 ms; (e) 2.5 ms; (f) 3.0 ms.

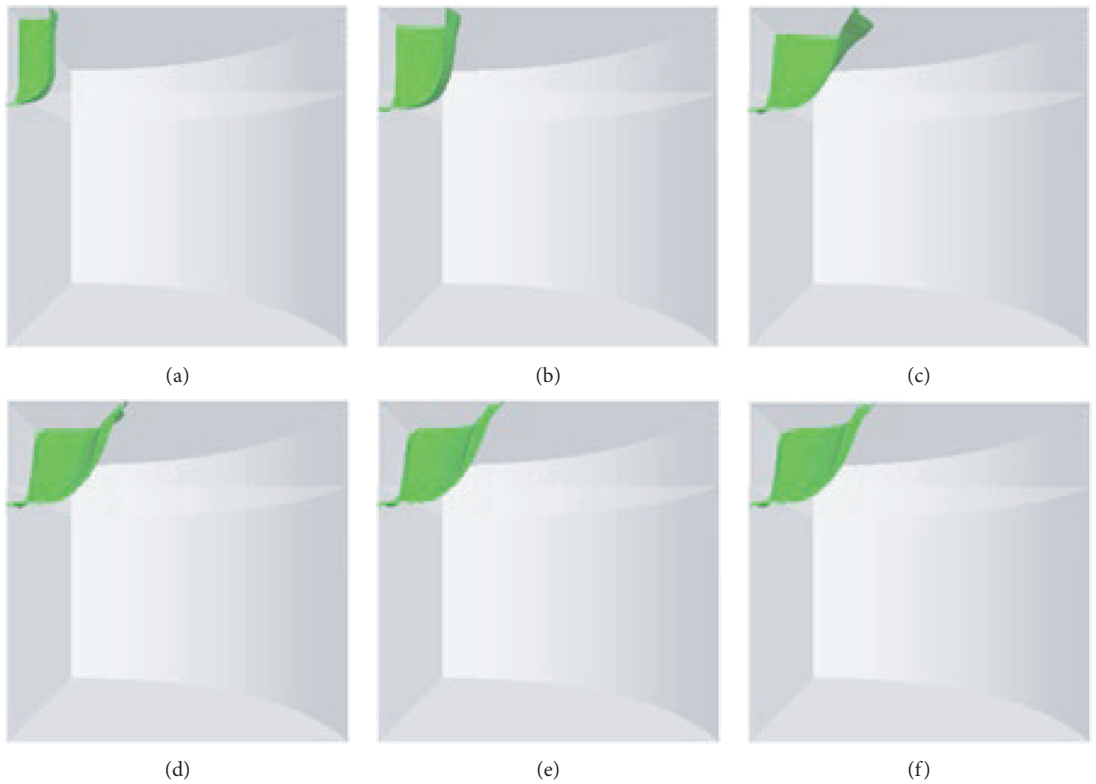

Figure 15: The development of rock mass fracture zone in head-up view: (a) 0.5 ms; (b) 0.8 ms; (c) 1.5 ms; (d) 2.0 ms; (e) 2.5 ms; (f) 3.0 ms.

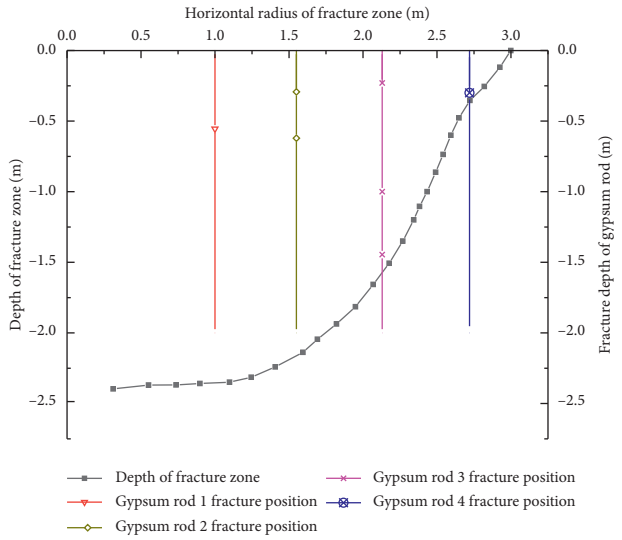

Figure 16: Comparison of the range of fracture zones in the blasting test.

that both the upper and lower parts of the No. 1 and No. 2 gypsum rods are broken, and the measured fracture depths of the lower parts of the gypsum rods are both greater than 2.0 m. Therefore, the borehole pre-embedded gypsum rod test can relatively accurately and intuitively reflect the critical fracture depth of the rock under the blasting load and thus obtain the range of the rock fracture zone.

5. Conclusions

This paper proposes a method that can accurately and directly obtain the range of the fracture zone of the rock slope under the blasting load. The basic principle of the method in which embedded test rods are drilled around the blast hole and subjected to blasting load is based on the reflection and transmission theory of the stress wave of different media interface. Based on the field blasting test and the numerical simulation presented in this study, the following conclusions can be drawn:

(1) Based on the closeness between the transmission coefficient of the stress wave through the test rod-rock interface and the ratio of the dynamic compressive strength of the test rod to the dynamic tensile strength of the rock, the fracture range of the test rod after blasting can be used as the range of the surrounding rock fracture zone after the slope blasting.

(2) In the field blasting test, the range of the surrounding rock blasting fracture zone conforms to the general distribution pattern of the surrounding rock fracture zone under blasting load.

(3) The relative error between the field blasting test results and the numerical analysis results in this paper is less than 18%, indicating that the proposed test method has a good accuracy. The test method described in this paper adopts shallow hole blasting, and this method is also applicable to deep hole blasting.

Data Availability

The data sets used to support the findings of this study are included within the article.

Conflicts of Interest

The authors declare that they have no conflicts of interest.

Acknowledgments

This work was supported by the National Natural Science Foundation of China (no. 51909192) and the Open Project of Engineering Research Center of Phosphorus Resources Development and Utilization of Ministry of Education (no. LKF202004).

References

[1] C. W. Livingston, "Fundamental concepts of rock failure," *Quarterly of the Colorado School of Mines*, vol. 51, no. 3, pp. 1–11, 1956.

[2] H. P. Rossmanith, K. Uenishi, and N. Kouzniak, "Blast wave propagation in rock mass-part I: monolithic medium," *Fragblast*, vol. 1, no. 3, pp. 317–359, 1997, in Chinese.

[3] X. Xia, *Study on damage characteristics and safety threshold of rock vibration by blast*, Ph.D. thesis, Institute of Rock and Soil Mechanics, Chinese Academic of Sciences, Wuhan, China, 2000, in Chinese.

[4] J. Dai, *Dynamic Behaviors and Blasting Theory of Rock*, Metallurgical Industry Press, Beijing, China, 2013, in Chinese.

[5] L. M. Taylor, E.-P. Chen, and J. S. Kuszmaul, "Microcrack-induced damage accumulation in brittle rock under dynamic loading," *Computer Methods in Applied Mechanics and Engineering*, vol. 55, no. 3, pp. 301–320, 1986.

[6] R. Yang, W. F. Bawden, and P. D. Katsabanis, "A new constitutive model for blast damage," *International Journal of Rock Mechanics and Mining Sciences & Geomechanics Abstracts*, vol. 33, no. 3, pp. 245–254, 1996.

[7] J. Chen, J. Zhang, and X. Li, "Rock blasting-induced damage zone under blasting excavation in a large underground chamber," *Journal of Central South University (Science and Technology)*, vol. 47, no. 11, pp. 3808–3817, 2016.

[8] B. J. Thorne, P. J. Hommert, and B. Brown, "Experimental and computational investigation of the fundamental," in *Mechanisms of Crater*ingSandia National Labs, Albuquerque, NM, USA, 1990.

[9] J. Lemaitre, "How to use damage mechanics," *Nuclear Engineering and Design*, vol. 80, no. 2, pp. 233–245, 1984.

[10] Y. Yang, Z. Shao, J. Mi, and X. Xiong, "Effect of adjacent hole on the blast-induced stress concentration in rock blasting," *Advances in Civil Engineering*, vol. 2018, Article ID 5172878, 13 pages, 2018.

[11] Z. L. Wang, Y. C. Li, and R. F. Shen, "Numerical simulation of tensile damage and blast crater in brittle rock due to underground explosion," *International Journal of Rock Mechanics and Mining Sciences*, vol. 44, no. 5, pp. 730–738, 2007.

[12] L. Liu and P. D. Katsabanis, "Development of a continuum damage model for blasting analysis," *International Journal of*

Rock Mechanics and Mining Sciences, vol. 34, no. 2, pp. 217–231, 1997.

[13] B. Mobaraki and M. Vaghefi, "Numerical study of the depth and cross-sectional shape of tunnel under surface explosion," *Tunnelling and Underground Space Technology*, vol. 47, pp. 114–122, 2015.

[14] J. H. Williams and C. D. Johnson, "Acoustic and optical borehole-wall imaging for fractured-rock aquifer studies," *Journal of Applied Geophysics*, vol. 55, no. 1, pp. 151–159, 2004.

[15] Y. Kanaori, "The observation of crack development around an underground rock chamber by borehole television system," *Rock Mechanics and Rock Engineering*, vol. 16, no. 2, pp. 133–142, 1983.

[16] K. J. Cunningham, "Application of ground-penetrating radar, digital optical borehole images, and cores for characterization of porosity hydraulic conductivity and paleokarst in the biscayne aquifer, Southeastern Florida, USA," *Journal of Applied Geophysics*, vol. 55, no. 1-2, pp. 61–76, 2004.

[17] S. Ray and S. Dauji, "Ground vibration attenuation relationship for underground blast: a case study," *Journal of the Institution of Engineers (India): Series A: Series A*.vol. 100, no. 4, pp. 763–775, 2019.

[18] Y. Fang, Z. Yao, and W. Gabriel, "Evaluating the impact of blast-induced damage on the rock load supported by liner in construction of a deep shaft: a case study of ventilation shaft of micangshan road tunnel project," *Advances in Civil Engineering*, vol. 2020, Article ID 9068345, 19 pages, 2020.

[19] X. Li, J. Chen, and Y. Li, "Research on blasting damage range and criterion of underground powerhouse in Xiluodu power stati," *Chinese Journal of Rock Mechanics and Engineering*, vol. 29, no. 10, pp. 2042–2049, 2010, in Chinese.

[20] Y. Hu, R. Li, X. Wu, G. Zhao, and Q. Zhang, "Blasting damage depth in layered jointed basalt before and after grouting," *Journal of Geotechnical and Geoenvironmental Engineering*, vol. 145, no. 3, Article ID 04018113, 2019.

[21] M. Pan, Y. Wu, and X. Shi, "Numerical simulation of deep hole blasting parameters in Fankou lead and zinc mine," *Mining Technology*, vol. 13, no. 5, pp. 87–89, 2013, in Chinese.

[22] X. Wang, "Study on damage range of rock mass under blasting impact," *Journal Engineering Geology*, vol. 22, no. 2, pp. 233–237, 2014.

[23] J. Yang, W. Lu, and M. Chen, "Determination of explosive load variation course of gun hole," in *Proceedings of the 2nd National Engineering Safety and Protection Academic Conference*, pp. 773–777, Beijing, China, August 2010, in Chinese.